JOURNAL OF GEOPHYSICAL RESEARCH: OCEANS, VOL. 118, 1–15, doi:10.1002/jgrc.20211, 2013

Lateral diffusivity from tracer release experiments in the tropical North Atlantic thermocline

Donata Banyte,[1] Martin Visbeck,[1] Toste Tanhua,[1] Tim Fischer,[1] Gerd Krahmann,[1] and Johannes Karstensen[1]

Received 18 December 2012; revised 17 April 2013; accepted 18 April 2013.

[1] Lateral diffusivity is computed from a tracer release experiment in the northeastern tropical Atlantic thermocline. The uncertainties of the estimates are inferred from a synthetic particle release using a high-resolution ocean circulation model. The main method employed to compute zonal and meridional components of lateral diffusivity is the growth of the second moment of a cloud of tracer. The application of an areal comparison method for estimating tracer-based diffusivity in the field experiments is also discussed. The best estimate of meridional eddy diffusivity in the Guinea Upwelling region at about 300 m depth is estimated to be $K_y = 500 \pm 200$ m^2 s^{-1}. The zonal component of lateral diffusivity is estimated to be $K_x = 1200 \pm 600$ m^2 s^{-1}, while areal comparison method yields areal equivalent zonal diffusivity component of $K_x^e = 1000 \pm 500$ m^2 s^{-1}. In comparison to K_y, K_x is about twice larger, resulting from the tracer patch stretching by zonal jets. Employed conceptual jet model indicates that zonal jet velocities of about 0.015 ± 0.005 m s^{-1} are required to explain the enhancement of the zonal eddy diffusivity component. Finally, different sampling strategies are tested on synthetic tracer release experiments. They indicate that the best sampling strategy is a sparse regular sampling grid covering most of the tracer patch.

Citation: Banyte, D., M. Visbeck, T. Tanhua, T. Fischer, G. Krahmann, and J. Karstensen (2013), Lateral diffusivity from tracer release experiments in the tropical North Atlantic Thermocline, *J. Geophys. Res. Oceans*, *118*, doi:10.1002/jgrc.20211.

1. Introduction

[2] Lateral dispersion of tracer in the ocean is a result of a complex interplay between a time-mean advection and mixing by eddies. In the coarse resolution climate models, the large-scale advection is well simulated, whereas eddy-driven transport must be parametrized, typically, as down-gradient diffusion with eddy diffusivity coefficient K. The extensive research on eddy-driven diffusion shows that eddy mixing has high-geographical variability, complex interaction with the mean flow, and can be highly anisotropic [e.g., *Kamenkovich et al*., 2009; *Rypina et al*., 2012; *Abernathey and Marshall*, 2013].

[3] The enhancement in eddy activity is found near strong currents, where eddies are driven by instabilities in the mean flow [e.g., *Gill et al*., 1974]. Such high-lateral mixing regimes are found near western boundary currents or Antarctic Circumpolar Current. Recently, however, it was observed that directly over an eastward mean flow eddy diffusivity coefficient can be actually smaller than on the flanks of the flow [e.g., *Abernathey et al*., 2010; *Ferrari and Nikurashin*, 2010]. Since eddy mixing is maximum when the eddies travel at the same speed as the mean flow, everywhere where velocity differences are large eddy mixing is suppressed. Hence, along the strong eastward current antarctic circumpolar current, eddy mixing is suppressed more than at the flanks of the flow. Furthermore, as eddies travel westward, eddy mixing in the mean westward flow is only slightly suppressed. The recent model study of tracer spread simulations in the velocity field observed from satellites have shown the large eddy mixing suppression in Antarctic Circumpolar Current region, but only weak suppression in the westward flow [*Abernathey and Marshall*, 2013].

[4] The tropical north-east Atlantic, our site of experiments, has weak mean flow conditions. In agreement with the ventilated thermocline theory by *Luyten et al*. [1983], the thermocline of eastern basins of tropical Atlantic and Pacific oceans can not be ventilated directly by the return flow of subtropical gyres. Instead, the regions are ventilated by the zonal eastward currents. In the tropical north-east Atlantic, the most pronounced eastward flowing currents extending through the thermocline are the north equatorial undercurrent (NEUC) and the northern branch of the north equatorial countercurrent (nNECC), located at about 5°N and 9°N, respectively [*Stramma et al*., 2005]. Both currents are thought to be part of the tropical system of alternating zonal jets. These jets are eddy-driven and are not reproduced by noneddy-permitting numerical simulations [e.g., *Rhines*, 1994; *Berloff et al*., 2009]. Nevertheless, they are clearly seen in the time-averaged zonal velocities in

[1]Physical Oceanography, GEOMAR, Helmholtz Centre for Ocean Research, Kiel, Germany.

Corresponding author: D. Banyte, GEOMAR, Helmholtz Centre for Ocean Research, Duesternbrooker Weg 20, Kiel D-24105, Germany. (dbanyte@geomar.de)

2169-9275/13/10.1002/jgrc.20211

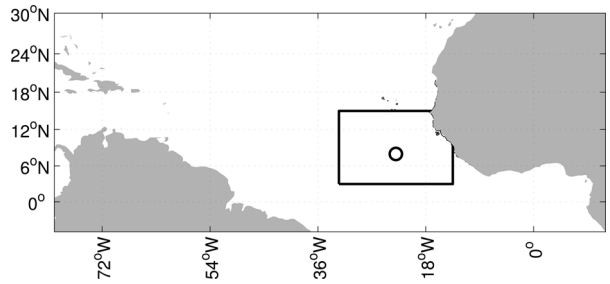

Figure 1. The guinea tracer release experiment (rectangle) and the tracer release position (circle).

observations [e.g., *Maximenko et al.*, 2005] as well as high-resolution ocean models [e.g., *Nakano and Hasumi*, 2005]. Hence, multiple alternating zonal jets must also be parametrized together with the eddy diffusion in coarse resolution ocean models.

[5] Alternating zonal jets make tracer dispersion highly anisotropic with zonal tracer diffusivity much larger than meridional [*Kamenkovich et al*., 2009; *Rypina et al*., 2012]. Partially anisotropy could be explained by the shear dispersion of the zonal jets [*Smith*, 2005]. However, *Rypina et al*. [2012], using simulated and observed trajectories of particle spreading, indicate that even when time-mean velocities of jets are removed, the eddy-only dispersion can still be highly anisotropic. Anisotropy seen in high-resolution model simulations of tracer spread was also reported by [*Eden and Greatbatch*, 2009], who suggest to use zonal and meridional components of eddy diffusivity in noneddy-permitting ocean models.

[6] In this study, we analyze the tracer spread from a large-scale tracer release experiment conducted in the northeastern tropical Atlantic thermocline (Figure 1). The guinea upwelling tracer release experiment (GUTRE) was performed in 2008 – 2010 with the injection cruise in 2008 and three tracer sampling cruises: 7, 20, and 30 months after injection [*Banyte et al*., 2012]. The integral timescales of the tracer used in this study are 20 and 30 months, and the spatial scales are about 2000 km in the zonal direction and 1000 km in the meridional direction. The zonal enhancement of tracer spread is attributed to both eddies and zonal jets. In general, in observational studies, it is particularly difficult to separate eddy-only tracer diffusion from the time-mean effect of alternating zonal jets. Furthermore, the large scales of tracer patch that span through almost the whole eastern basin of tropical North Atlantic yield integrative diffusivities, where not only several alternating zonal jets contribute, but also various mixing regimes are accounted for.

[7] The eastern basin of tropical North Atlantic is a region of very low-oxygen concentrations at about 400 m depth. There, the low-oxygen conditions at the subsurface forms as a consequence of weak circulation, long water renewal pathways, which are mainly eastward flowing currents NEUC and nNECC, and high-biological oxygen consumption rates at the subsurface. The zonal jets in combination with mesoscale eddies play an important role in transporting oxygen rich waters into the region [*Brandt et al*., 2010]. In the wake of significant deoxygenation observed in the oxygen minimum zones (OMZs) [*Stramma et al*., 2008], the estimation of lateral eddy diffusivity and zonal advection is required to answer whether the zones would expand or contract in the future. *Fischer et al*. [2012], after computing the diapycnal oxygen influx and comparing it with the conceptual oxygen consumption model by *Karstensen et al*. [2008], suggest that as much as about 70% of the total oxygen supply is delivered by lateral pathways. Considering large contribution of lateral mixing for the oxygen balance in OMZs, reliable estimates of lateral diffusivity are required.

[8] This paper is organized as follows: section 2 describes the three methods applied to the tracer patch to estimate the lateral eddy diffusivity coefficient, section 3 lists three data sets, one of which is observational and two are modeled tracer releases. Finally, the results are given in section 4 and discussed in section 5.

2. Methods

[9] In this study, three methods are employed to estimate lateral eddy diffusivity. All analyze a tracer distribution after spreading from a point source and estimate an average lateral diffusivity at a specific time. Two methods describe the growth of the second moment of a cloud of tracer and differ only in the way the second moment is estimated: either from a Gaussian distribution fit to the data [e.g., *Ledwell et al*., 1998], or by the computation of the centered second moment of particles weighted by the amount of tracer [e.g., *Sundermeyer and Lelong*, 2005; *Klocker et al*., 2012]. Both methods yield the zonal and meridional components of lateral diffusivity. The third method explores how areas of tracer concentration classes in the tracer patch increase over time in comparison with a tracer patch described by a simple two-dimensional diffusion. The isotropic diffusivity coefficient that best fits the areal spread of the observed tracer patch is called areal equivalent diffusivity.

[10] All three methods applied to estimate lateral eddy diffusivity rely on the assumption that on large scales, the second moment of the tracer cloud increases linearly in time [*Garrett*, 1983]. Along-isopycnal two-dimensional dispersion (variance) can then be described by Fick's diffusion: $\mathrm{var}(C)|_{x,y} = 2K_{x,y}t$, where C is the tracer concentration, i.e., tracer column inventory in units of mol m^{-2}, and K_x and K_y are zonal and meridional components of lateral eddy diffusivity. The areal equivalent diffusivity, assumed to be isotropic, is labeled as K_e.

2.1. Second Moment of a Cloud of Tracer

2.1.1. Gaussian Fit Method

[11] The growth of the second moment of a cloud of tracer can be estimated by fitting a Gaussian distribution to the tracer patch: $\mathrm{var}(C)|_{x,y} = \sigma^2_{x,y}$, where σ_x and σ_y represent standard deviations of the Gaussian distribution along zonal and meridional directions, respectively. The method was, for example, applied in the North Atlantic tracer release experiment (NATRE) [*Ledwell et al*., 1998]. In this study, to obtain the mean lateral diffusivity estimates, we first averaged the tracer patch either zonally or

meridionally, and then applied a 1-D Gaussian fit to each of the mean curves. In the tropical Atlantic, where zonal jets elongate the tracer patch in x direction, the zonal component (σ_x) is expected to be much larger than its meridional counterpart (σ_y). The results of this technique will be labeled G (for Gaussian fit) in the following.

2.1.2. Weighted Particle Method

[12] An alternative way to estimate the second moment of a cloud of tracer is via the weighted particle dispersion. In the observations, this means that each tracer measurement at a station is represented as a particle with the weight equal to the vertical tracer concentration integral (i.e., tracer column inventory). The weighted particle dispersion in the zonal direction can be written as

$$\sigma_x^2 = \frac{\sum_{i=1}^{N} (x_i - x_c)^2 C(x_i)}{\sum_{i=1}^{N} C(x_i)},$$

[13] where N is the number of tracer particles, $C(x_i)$ is the weight (tracer column inventory), and x_c is the center of mass in the zonal direction of the tracer patch:

$$x_c = \frac{\sum_{i=1}^{N} x_i C(x_i)}{\sum_{i=1}^{N} C(x_i)}.$$

[14] The results of this technique will be labeled P for Particle method.

[15] Two ways to compute the second moment of a tracer patch are compared because it is expected that the Gaussian fit method is less sensitive to gaps in the data and to possible outliers. On the other hand, the assumption that a tracer patch distribution is Gaussian might be too restrictive and therefore the fit is less robust and associated uncertainties are larger.

2.2. Areal Equivalent Diffusivity

[16] The areal equivalent diffusivity (K_e) is computed after a new isotropic tracer patch is constructed, which by the areal distribution of tracer concentration classes represents the observed tracer patch, but with streakiness and anisotropy removed.

[17] Depending on the sampling frequency, either 50 or 20 tracer concentration classes are chosen ranging from zero to the maximum concentration in the studied tracer patch. The area-concentration function ($A(C)$) is described as:

$$A(C) = \sum_{C_{\max}}^{C} a(c),$$

[18] where $C_{\max}$ is a maximum tracer concentration found in the patch, $a(c)$ is the area of c concentration class. Hence, function $A(C)$ is a cumulative area distribution of tracer concentration classes; it describes the total area of the tracer patch with higher concentrations than a chosen limit (C). The inverse of the function indicates the total amount of tracer found in the chosen area. However, the inverse function is more difficult to compute in field experiments.

[19] After constructing the area-concentration function for the tracer patch, we compare it with a range of functions computed for an idealized tracer patch described by Fickian diffusion with an isotropic diffusion coefficient. The best fit is searched for in the range of isotropic diffusivities (K_e) from 140 to 1560 m^2 s^{-1} with a step of 20 m^2 s^{-1}. A rather large diffusivity step is chosen because the uncertainty of the estimates is expected to be much larger for the sparsely sampled tracer patch.

[20] Considering that zonal enhancement of tracer mixing is not only due to eddy effect, but also due to the time-mean advection by zonal jets, the areal equivalent diffusivity helps to evaluate the effective tracer mixing in zonal direction, irrespectively of the geometric shape of the tracer patch. The tracer distribution can significantly deviate from the Gaussian distribution which affects the estimate of zonal lateral diffusivity component. Using the areal equivalent diffusivity estimate, the equivalent zonal diffusivity component can be computed as $K_{xe} = K_e/K_y$.

3. Data

[21] The main objective of this study is to estimate lateral eddy diffusivity from the observations of the tracer release experiment, where tracer sampling was irregular and spatially limited. In order to estimate the uncertainties of our results, two synthetic tracer releases were modeled and analyzed.

[22] As a result, three data sets were used in this study: (1) from a synthetic tracer release in a conceptual jet model, (2) from a synthetic particle release in a high-resolution ocean circulation model, and (3) from the observations of the tracer release experiment conducted in the northeast tropical Atlantic in the Guinea upwelling region. The details of these experiments are given later.

3.1. Conceptual Jet Model

[23] The tracer release experiment is simulated using a conceptual jet model, which is described by the advection-diffusion equation as follows:

$$\frac{\partial C}{\partial t} + u\frac{\partial C}{\partial x} + v\frac{\partial C}{\partial y} = K_x\frac{\partial^2 C}{\partial x^2} + K_y\frac{\partial^2 C}{\partial y^2}, \quad (1)$$

where C is tracer concentration and the value of the isotropic eddy diffusivity coefficient is chosen as $K_x = K_y = 400$ m^2 s^{-1}. The nondivergent velocity field is defined as $u = -\partial\psi/\partial y$ and $v = \partial\psi/\partial x$, where the streamfunction ψ is

$$\psi = u_0 \sin\left(2\pi y/l_y\right)\sin\left(2\pi x/l_x\right).$$

[24] Here velocity at the center of the zonal jet was chosen to be $u_0 = 0.01$ m s^{-1}, while l_x and l_y represent the period of periodically alternating jets in the zonal and meridional directions, respectively (Figure 2). In the boundary range of $x = [3°\text{W}43°\text{W}]$ and $y = [12°\text{S}28°\text{N}]$, we chose $l_x = 40°$ and $l_y = 4°$. In this way, there were twenty stacked zonal jets in the domain. The tracer release position was either at 8°N 23°W or at 7°N 23°W

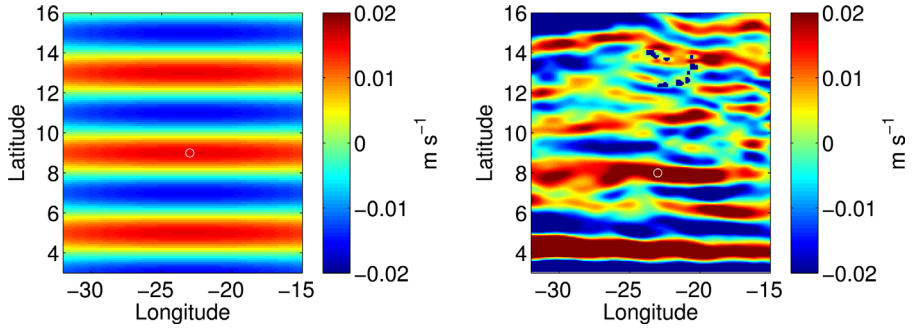

Figure 2. Velocities in a conceptual jet model (left) and in studied subregion of FLAME model (right). In the latter, 53 instanteous velocity fields were averaged, each 1 week apart.

corresponding to either the location directly between the two jets or in the middle of a jet.

3.2. General Circulation Model (FLAME)

[25] The particle releases were simulated using output of the high-resolution ($\frac{1^\circ}{12}$) ocean model FLAME (Family of Linked Atlantic Model Experiments) [*Dengg et al*., 1999]. FLAME is based on a modified version of the *z*-coordinate modular ocean model (MOM2) [*Pacanowski et al*., 1995] and has been set up for the Atlantic Ocean between 70°N and 18°S [e.g., *Eden and Böning*, 2002]. The particle release simulations used a horizontal grid of $\frac{1^\circ}{12}$ and 45 vertical levels with a resolution decreasing toward greater depths. More detailed information on the model configuration is given in the work of *Hüttl-Kabus and Böning* [2008].

[26] The model has been used previously for several studies in the Tropical Atlantic, e.g., in the works of *Hüttl and Böning* [2006], *Kirchner et al*. [2009], and *Brandt and Eden* [2005]. The study of *Kirchner et al*. [2008] compared model results with observations, indicating realistic model behavior with respect to the observed mean tracer transport and its variability in the western tropical Atlantic. Furthermore, FLAME reproduces the zonal current bands reasonably well (Figure 2), even though modeled velocities of the current bands fall below observed velocities at greater depths [*Stramma et al*., 2005].

[27] The tracer patch was represented by an ensemble of particles passively transported by the FLAME velocity output at a depth of 250 m [*Fischer*, 2007]. A typical particle release simulation consisted of about 10,000 particles whose position and velocities were traced over almost 30 months (132 weeks). Overall, 53 particle releases were used in this study, each of them starting at the same position of 8°N 23°W, but a week apart in response to different instantaneous flow conditions. Examples of two, out of 53, particle release simulations at time intervals of 20 and 30 months after the release are shown in Figure 3. The chosen time periods correspond to the two surveys of the observed tracer release experiment in the northeastern tropical Atlantic (GUTRE).

3.3. The Guinea Upwelling Tracer Release Experiment (GUTRE)

[28] The GUTRE started with 92 kg of the tracer halocarbon trifluoromethyl sulfur pentafluoride (CF_3SF_5) being released at 8°N 23°W in April 2008. The release isopycnal was $\sigma_\Theta = 26.88$ kg m^{-3}, corresponding to a depth of about 350 m. The spreading tracer was sampled during three subsequent surveys: 7, 20, and 30 months after the tracer release. The experiment was primarily designed to estimate diapycnal diffusivity, results of which are described by *Banyte et al*. [2012]. In this study, however, we estimate the large scale, time integrated, isopycnal eddy diffusivity. As the earlier survey revealed a very streaky tracer patch, we analyzed only the surveys performed 20 and 30 months after tracer release, where tracer patch extent reached more than 1000 km (Figure 4) and patches were well spatially homogenized.

[29] Concentration maps of tracer column integrals (Figure 4) were interpolated using Gaussian weights, where the meridional radius of influence was chosen arbitrarily to be 25 km (first survey) and 100 km (second and third surveys); correlation scales are expected to be larger than 100 km in the 20–30 months old tracer patch [*Ledwell et al*., 1998]. The zonal radius of influence was twice as large. Furthermore, zeros were assigned at a cut-off radius distance from the nearest cast position; the cut-off radius being two times the radius of influence.

[30] A visual inspection of the tracer patch during the second and third surveys indicates that the center of mass of the tracer patch has not significantly shifted with respect to the tracer release position (Figure 4). The estimated center of mass for each of the two surveys deviates about 1.5° from the release position. The entrapment of the tracer in the region agrees with the notion of the shadow zone, i.e., a region of weak ventilation. The zonal extent of the tracer patch is larger than the meridional extent in both surveys. Furthermore, large tracer column inventories found at 28°W during the 30 months survey indicate that the patch extended westward beyond the farthest sampled longitude.

3.4. Sampling Strategies

[31] In this study, several tracer sampling grids are used. The fine resolution grid applied for the modeled data is $0.3^\circ \times 0.3^\circ$. In the case of the particle release in the FLAME model, we converted particles to tracer concentrations by counting the number of particles within the grid boxes. A fine sampling resolution of 0.3° is not possible to achieve in the field experiments because of time limitations. Therefore, lower sampling resolution strategies were tested. For the modeled tracer releases, the partial data set was constructed by resampling the original fine resolution grid using $1^\circ \times 1^\circ$ grid, $2^\circ \times 2^\circ$ grid, or by applying the

exact sampling strategy of the GUTRE. To avoid the confusion between the results computed using different sampling strategies, the notation was added: f for the fine sampling resolution of 0.3°, 1°, and 2° for the low-sampling resolution by the regular sampling grid, and g for the exact sampling strategy of the GUTRE.

[32] Lateral diffusivities were also computed along separate transects of the tracer patch. For the fine resolution data the transects were computed along the cross section of each longitude and latitude 0.3° apart, for the sparse resolution—each 1° or 2° apart. In the GUTRE observations, only a number of well sampled transects are available.

4. Results

4.1. Conceptual Jet Model

[33] The tracer release is simulated in the idealized velocity field with parametrized isotropic eddy diffusivity of $K_x = K_y = 400$ m^2 s^{-1} and overlaid alternating zonal advection with the meridional period of 4° and maximum velocity in the middle of the jets of 0.01 m s^{-1}. The tracer spread is described by equation (1). There are two examples compared: when the tracer is released in the middle of the zonal jet and released between the zonal jets.

4.1.1. Full Data set

[34] The Gaussian fit and weighted particle methods yield similar mean eddy diffusivity estimates in zonal (K_x^f) and meridional (K_y^f) directions. Furthermore, the meridional result corresponds well with the imposed eddy diffusivity in the model of 400 m^2 s^{-1}, the difference being only about 10 m^2 s^{-1} (Table 1). The zonal component (K_x^f) affected by the zonal advection is, on the other hand, at least three times larger (about 1300 m^2 s^{-1}).

[35] The larger zonal lateral diffusivity component is manifestation of shear dispersion by the simulated jets, which increase tracer gradients and consequently mixing. The enhancement of mixing in zonal direction is seen from equivalent area diffusivity (K_e^f). K_e^f estimate for the two

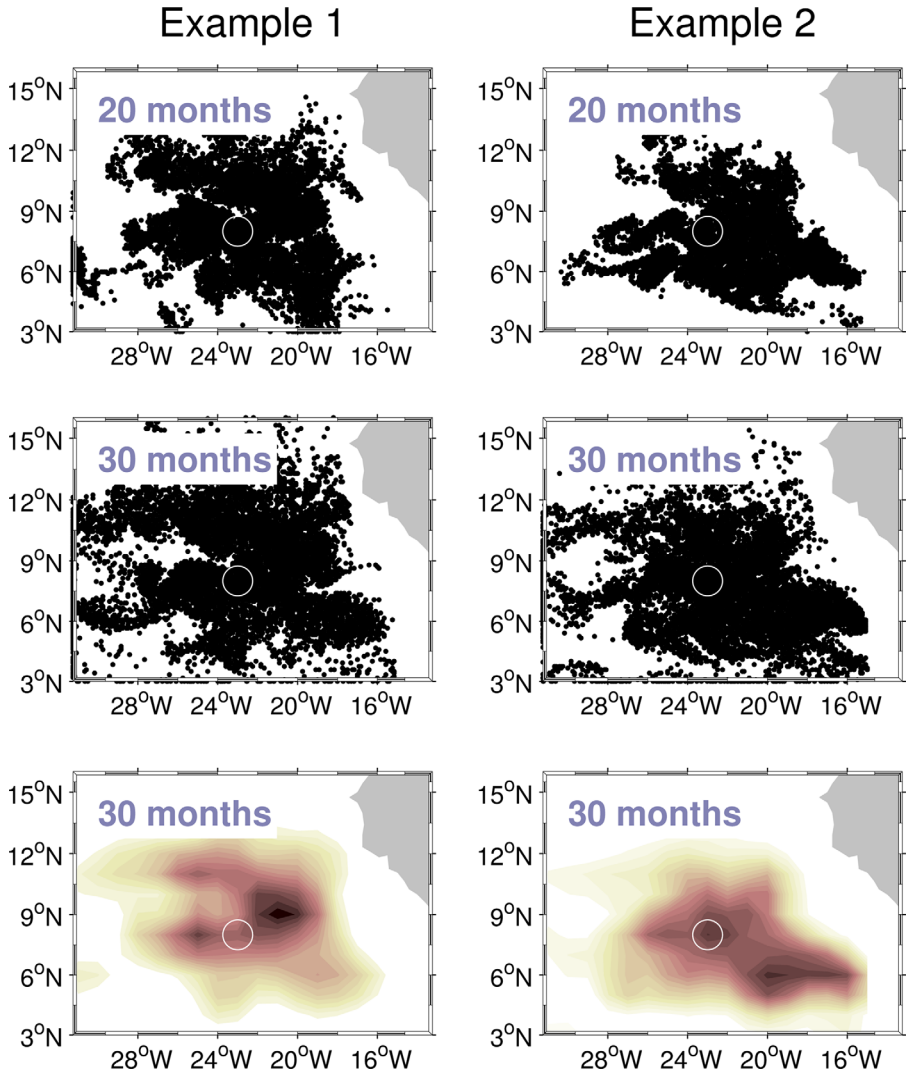

Figure 3. Examples of two particle releases at 250 m depth in high-resolution ocean model FLAME at time intervals: 20 and 30 months after the tracer release. (Bottom) the same examples at 30 months, but particles are converted to concentrations using fine grid of 0.3° and interpolated with Gaussian weights, same as for GUTRE data.

Table 1. Eddy Diffusivities for the Two Examples (Tracer Release in the Middle of the Jet (MJ) or between the Jets (BJ)) of Synthetic Tracer Release in a Conceptual Jet Model Using a Full Data Set and Sampling Grids of 1° or 2°[a]

	Full		1°		2°	
	MJ	BJ	MJ	BJ	MJ	BJ
K_{xP} (m^2 s^{-1})	1230	1300	1229	1298	1246 ± 12	1315 ± 12
K_{xG} (m^2 s^{-1})	1410	1510	1411	1506	1434 ± 16	1515 ± 16
K_{yP} (m^2 s^{-1})	410	410	408	407	408 ± 1	408 ± 1
K_{yG} (m^2 s^{-1})	410	410	413	411	415 ± 2	414 ± 2
K_e (m^2 s^{-1})	720	780	720(±0)	800 ± 20	720 ± 20	790 ± 20

[a] K_{xP} and K_{yP} are eddy diffusivities from weighted particle method, K_{xG} and K_{yG}—from Gaussian fit method, and K_e is an areal equivalent lateral diffusivity.

examples is about $K_e^f = 750$ m^2 s^{-1} (Table 1). Taking into account zonal and meridional components of lateral diffusivity given above, we get that $\left(K_e^f\right)^2$ almost equal to $K_x^f K_y^f$, or equivalent zonal diffusivity component is about 1400 m^2 s^{-1} and thus close to K_x^f estimate. From this we conclude that in the two examples the zonal jets do not simply stretch the tracer patch, but enhance mixing in the zonal direction.

[36] Additionally, we employ the Gaussian fit and weighted particle methods to estimate diffusivity coefficients along each longitudinal or latitudinal transect of the gridded tracer patch. The transect analysis shows that K_x^f and K_y^f estimates vary significantly (Figures 5c–5f). As the tracer patch is constantly advected by the alternating mean flow, the tracer stays longer at some places than at others. For example, K_x^f differs by at least three times (K_y^f varies even up to five times) from the center of the patch to the boundaries. We conclude that diffusivity estimates computed from separate transects have large uncertainties.

4.1.2. Partial Data Set

[37] Next, we check how diffusivity estimates change when sparser sampling strategy is used to sample the tracer patch. The tracer field was partially sampled using a sparse regular grid of 1° or 2°. All three methods were found to be robust enough to recover the diffusivity coefficients in the range of uncertainties (Table 1). To evaluate the uncertainty of diffusivity coefficients using a sparse regular grid, we resampled a fine grid field a number of times by shifting the 1° or 2° sampling grid over the fine grid. The two standard deviations of the results were chosen as uncertainty ranges for diffusivity coefficients. Overall, the uncertainty was slightly increasing with the sparser grid. However, even with the sampling grid of 2°, the uncertainty of the estimates is small: often only 1% of the value.

[38] With the sparse sampling of the 2° grid, the number of stations required to cover the full tracer patch in the two examples are about 140. The rule of the thumb is that about 80 measurement casts spaced over regular 2° grid require about a month to complete. Here it is taken into account that the ship driving speed is about 10 km and the time spent over a measurement cast is about 1.5 h. Hence, to cover a full tracer patch is a challenge for an open ocean survey of about 1 month length.

[39] Decreasing the size of the studied area, however, significantly affects the mean eddy diffusivity estimates. A sampling area enclosing about 90% of the total tracer amount results in about 10% deviation in the diffusivity estimate. This area can be covered with about 80 stations using a sparse 2° sampling grid. In comparison, when only 50% of the total tracer amount is found within the sampled patch, the eddy diffusivity estimates ($K_x^{2^\circ}$ and $K_y^{2^\circ}$) deviate about 50% from the fine sampling resolution estimates (K_x^f and K_y^f).

[40] Similar results are achieved with the sampling grid of 1°. The finer sampling grid requires about twice as much stations to cover the same area, however the deviations from the fine grid estimates (K_x^f and K_y^f) do not improve if the area coverage is kept the same (Figure 6). We thus conclude that both Gaussian fit and weighted particle methods both yield good eddy diffusivity results for the homogeneous tracer patch as long as a large enough region is sampled.

4.2. General Circulation Model (FLAME)

[41] The uncertainty of the eddy diffusivity estimates and the best tracer patch sampling strategy might be different when applied to a more realistic example of the tracer patch evolution. The tracer released as a cloud of particles in the high-resolution ocean circulation model (FLAME) allows to test the performance of each of the three eddy

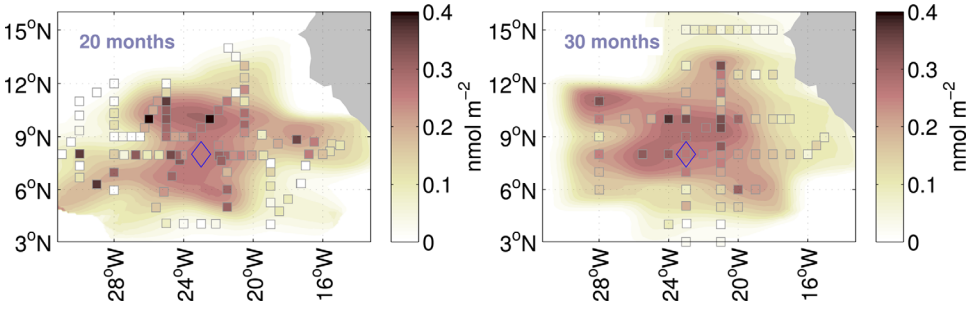

Figure 4. Horizontal tracer patch distribution during three surveys: (left) in December 2009 (20 months after tracer release) and (right) in October–November 2010 (30 months after tracer release). The color of the squares represents the tracer column integral; the same color bar applies to the filled contours. The blue diamond at 8°N, 23°W marks the tracer injection position, but the symbol is larger than the 20 km by 20 km area of the injection.

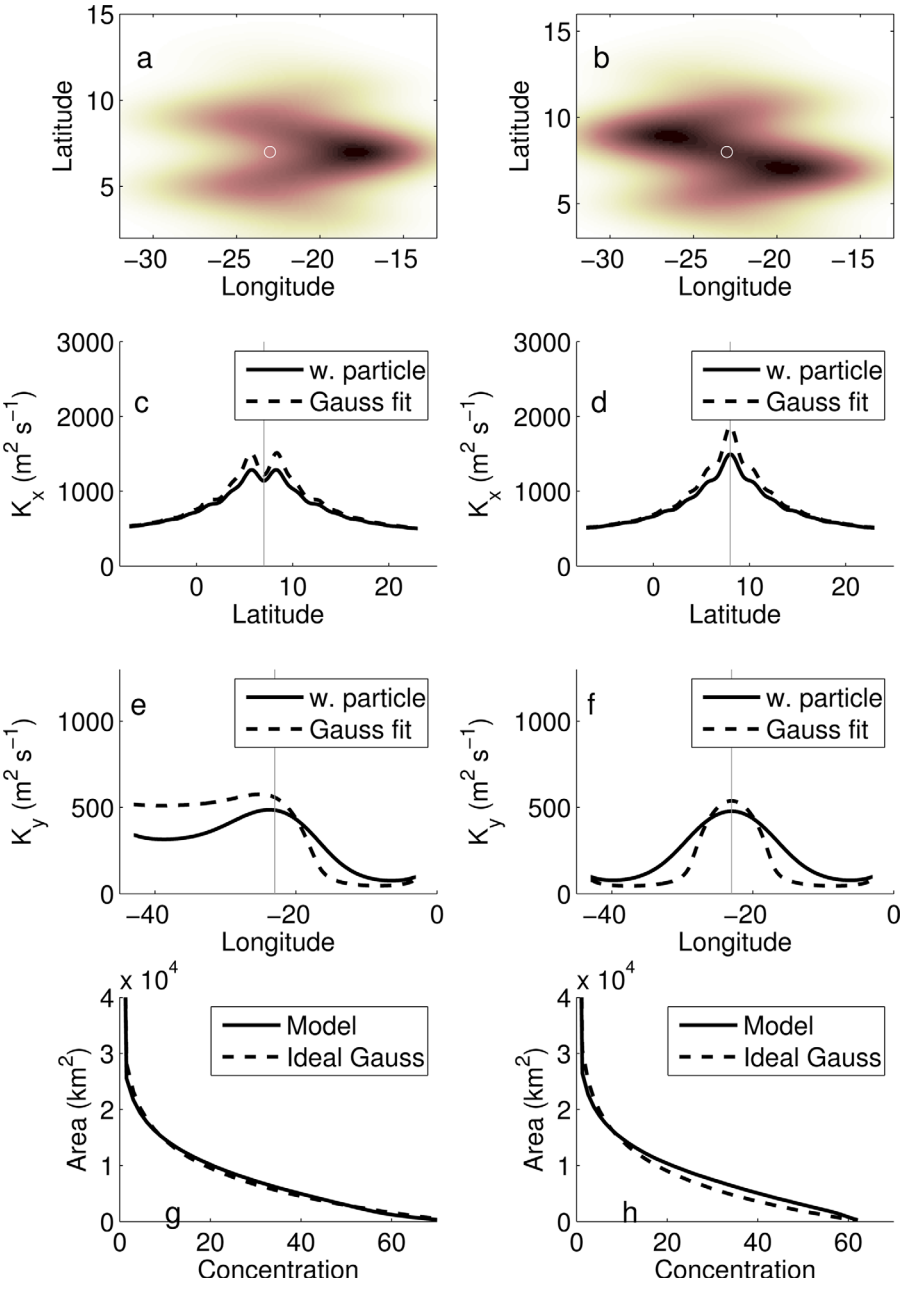

Figure 5. Two examples of synthetic tracer release in a conceptual jet model at 30 months, where a tracer is released in (a) the middle of the zonal jet, (b) in between of two zonal jets. The tracer release position is marked by a white circle. (c and d) The zonal and (e and f) meridional components of the eddy diffusivity are computed along each transect line. (g and h) Cumulative area-concentration function computed for the synthetic tracer release (thick black line) and its best fit computed for the isotropic Gaussian distribution (dashed line).

diffusivity computation methods on less homogeneous tracer field.

4.2.1. Full Data Set

[42] Eddy diffusivity was first computed with the full data set and fine grid of 0.3° for each of the 53 synthetic particle releases in FLAME model (Figure 7). The eddy diffusivity is not constant over time; both Gaussian fit and weighted particle methods result in noisy estimates at the early stages of tracer patch development, and overall show a tendency to increase with time. However, after about 20 months the increase slows down and the estimates converge. A slight increase of lateral diffusion estimates even after about 20 months indicate a slightly superdiffusive regime in the FLAME model in the studied region. It means that dispersion of particles grows faster than linear in time. Nevertheless, because deviation from the diffusive regime is small, and because FLAME model results are merely used to test the methods and various sampling strategies, we assume a constant lateral diffusivity in FLAME model after 20 months. Hence, averaged over the time period of

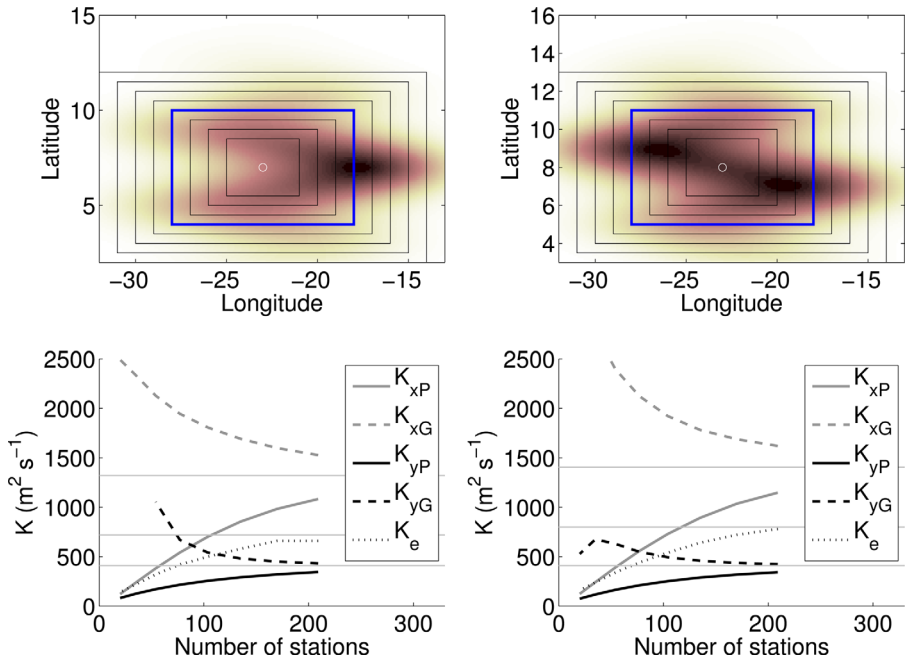

Figure 6. Eddy diffusivities versus the number of stations for the same two examples as in Figure 5, where a tracer is released in (left) the middle of the zonal jet and (right) in between of two zonal jets. The sampling grid is 1°. The boundaries of the minimum size regions resulting in estimate deviations of less than 50% are marked in blue (top). Three parallel gray lines, from top to bottom, indicate the mean estimates of the full data set of K_x, K_e, and K_y, respectively. Here K_{xP} and K_{yP} are eddy diffusivities from the weighted particle method, K_{xG} and K_{yG}—From the Gaussian fit method, and K_e is an areal equivalent lateral diffusivity.

20–30 months (90–132 weeks) and combining the results of the two methods, the mean lateral diffusivity is obtained for the FLAME model: $K_x^f = 870 \pm 100$ m^2 s^{-1}, and $K_y^f = 320 \pm 30$ m^2 s^{-1} (see also Table 2). Here again zonal diffusivity component is about 2.5 times larger than meridional.

[43] The areal equivalent lateral diffusivity estimates for each of the 53 particle release experiments behave similarly over time: are increasing at earlier times, but become almost stable after about 20 months (Figure 8). The noisy estimates at the early times of up to 9 months after the release were omitted from Figure 8; the areal comparison method yields a large noise in the early estimates, when only very high- or very low-tracer concentrations are observed. Averaged over the time period of 20–30 months (90–132 weeks), the mean estimate is $K_e^f = 335 \pm 21$ m^2 s^{-1}. Here, differently than in the conceptual jet model experiments, K_e^f estimate is relatively small, and more similar to the meridional lateral diffusivity component (K_y^f). Consequently, $\left(K_e^f\right)^2 \ll K_x^f K_y^f$, and areal equivalent zonal diffusivity component (K_{xe}) is only about 350 m^2 s^{-1}. Hence, in the FLAME model, the well-developed tracer patch evolves similarly to the tracer patch of isotropic Gaussian distribution with a diffusion coefficient close to K_y^f. We conclude that modeled zonal jets, variable in position and in strength, only geometrically deform the patch without significantly increasing mixing in zonal direction.

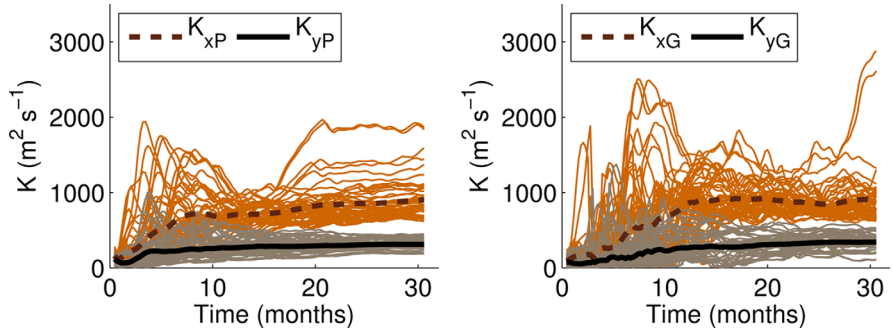

Figure 7. Zonal (K_x) and meridional (K_y) components of eddy diffusivity estimated at each 1 week time interval for each of the 53 different tracer releases in FLAME model and their mean. The estimates are computed either using weighted particle method (left figure, marked by *P*), or Gaussian fit method (right figure, marked by *G*).

Table 2. Eddy Diffusivities in FLAME Model, Either Averaged Over 53 Runs and the Time Period of 20–30 Months (87–132 Weeks), or Computed for the Two Examples and at the Time Period of 30 Months (132 Weeks)[a,b]

	Av. 53 runs	Ex 1			Ex 2		
	Full	Full	1°	2°	Full	1°	2°
K_{xP} ($m^2\ s^{-1}$)	860 ± 76	1270	1410 ± 150	1340 ± 370	750	780 ± 100	770 ± 200
K_{xG} ($m^2\ s^{-1}$)	880 ± 60	860	1050 ± 370	940 ± 620	790	800 ± 170	780 ± 400
K_{yP} ($m^2\ s^{-1}$)	305 ± 19	450	440 ± 50	450 ± 120	350	360 ± 60	350 ± 120
K_{yG} ($m^2\ s^{-1}$)	330 ± 28	500	430 ± 170	460 ± 340	420	430 ± 130	420 ± 230
K_e ($m^2\ s^{-1}$)	335 ± 21	490	500 ± 70	490 ± 110	360	370 ± 60	370 ± 140

[a]For the two examples, the diffusivities are computed for the full data set, or after the tracer patch was sampled using the regular sampling grid of 1° or 2°.

[b]K_{xP} and K_{yP} are eddy diffusivities from weighted particle method, K_{xG} and K_{yG}—from Gaussian fit method, and K_e is an areal equivalent lateral diffusivity.

4.2.2. Partial Data Set

[44] The tracer patch evolution in FLAME model is less homogeneous than in the synthetic tracer release in a conceptual jet model. We chose two random example runs out of 53 to explore the differences in diffusivity estimates with the sampling grid of 1° and 2° at a time period of 30 months (Figure 9). The diffusivity estimates in one example are similar to the ensemble mean, while in the other they are slightly larger (Table 2).

[45] Both coarse sampling strategies yield results deviate little from the fine grid diffusivity estimates. The uncertainties for the 2° sampling grid are about twice as large as for the 1° grid. Furthermore, the Gaussian fit method yields almost twice as large uncertainties and is associated with the additional error of the fit when the profiles deviate from the Gaussian distribution. Overall, the uncertainty of the zonal diffusivity estimates ($K_x^{1^\circ}$ and $K_x^{2^\circ}$) is found in the range of 300 $m^2\ s^{-1}$, while about 100 $m^2\ s^{-1}$ for the meridional estimates ($K_y^{1^\circ}$ and $K_y^{2^\circ}$) (Table 2). The uncertainty ranges are similar when computed for other examples of the 53 experiments.

[46] In both examples the areal equivalent lateral diffusivity closely agrees with the meridional estimate. Moreover, even using a sparse 2° grid the method recovers the estimates of the full data set within the uncertainty range of about 100 $m^2\ s^{-1}$. Hence, the method is robust enough to yield relatively good estimates with the sparse sampling grid even for the less homogeneous tracer patches of the FLAME model.

[47] The transect analysis of the two examples was carried out after the patches were sampled with 1° grid (Figure 9). The analysis shows a large variability of the $K_x^{1^\circ}$ and $K_y^{1^\circ}$ estimates along the transects. Despite the large variability, the transects near the release site, where the tracer is expected to linger the longest, yields the result closer to the fine grid and full field estimates. Hence, when lateral diffusivity estimates must be judged from several transects alone, the ones near the center of mass of the tracer patch, in this case, near the release site, must be chosen.

[48] In addition to reducing the sampling frequency, the smaller sampled region can help to limit the number of stations required to cover the region. The reduction of the sampled area, however, significantly increases the deviation of the estimates (Figure 10). Here the two examples are analyzed with the 1° sampling grid. When the sampled region covers about 50 – 70% of the total amount of the released tracer, the diffusivity estimates deviate about 50% from the full field estimates. A similar conclusion can be drawn from the 2° sampling strategy. We conclude that in the field experiments the coarse grid of 2° yields good diffusivity results as long as most of the tracer patch is sampled (>90%).

4.3. Guinea Upwelling Tracer Release Experiment

[49] The 20 and 30 months surveys of GUTRE were analyzed in this study. We used irregularly sampled data either directly to compute the estimates, or after horizontally interpolating with Gaussian weights (contours in Figure 4). The interpolation procedure is described in section 3.3.

[50] Meridional eddy diffusivity estimates, in the noninterpolated data analysis, agree well between the two surveys (Table 3), the average estimate being $K_y^{NI} = 320\ m^2\ s^{-1}$. The zonal diffusivity component (K_x^{NI}), on the other hand, is estimated to be much smaller in the third survey than in the second survey. The difference is a consequence of the limited westward extent of the third survey; the whole western part of the tracer patch was not sampled in the third survey (Figure 4). In comparison, the second

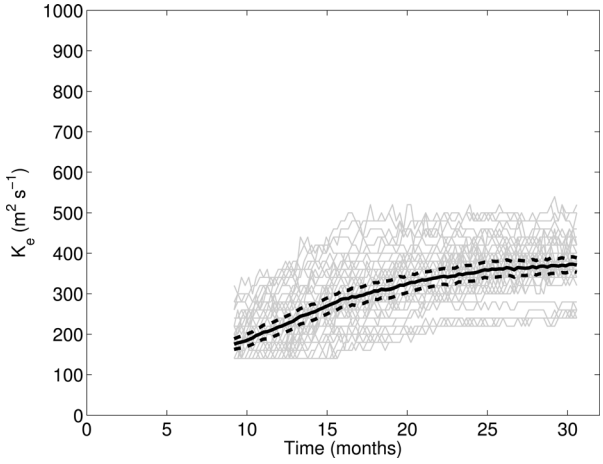

Figure 8. Areal equivalent lateral diffusivity estimated at each 1 week time interval for each of the 53 different tracer releases in FLAME model and their mean (black solid line). The error bars (black dashed line) are computed as a standard error at each time period of all 53 runs.

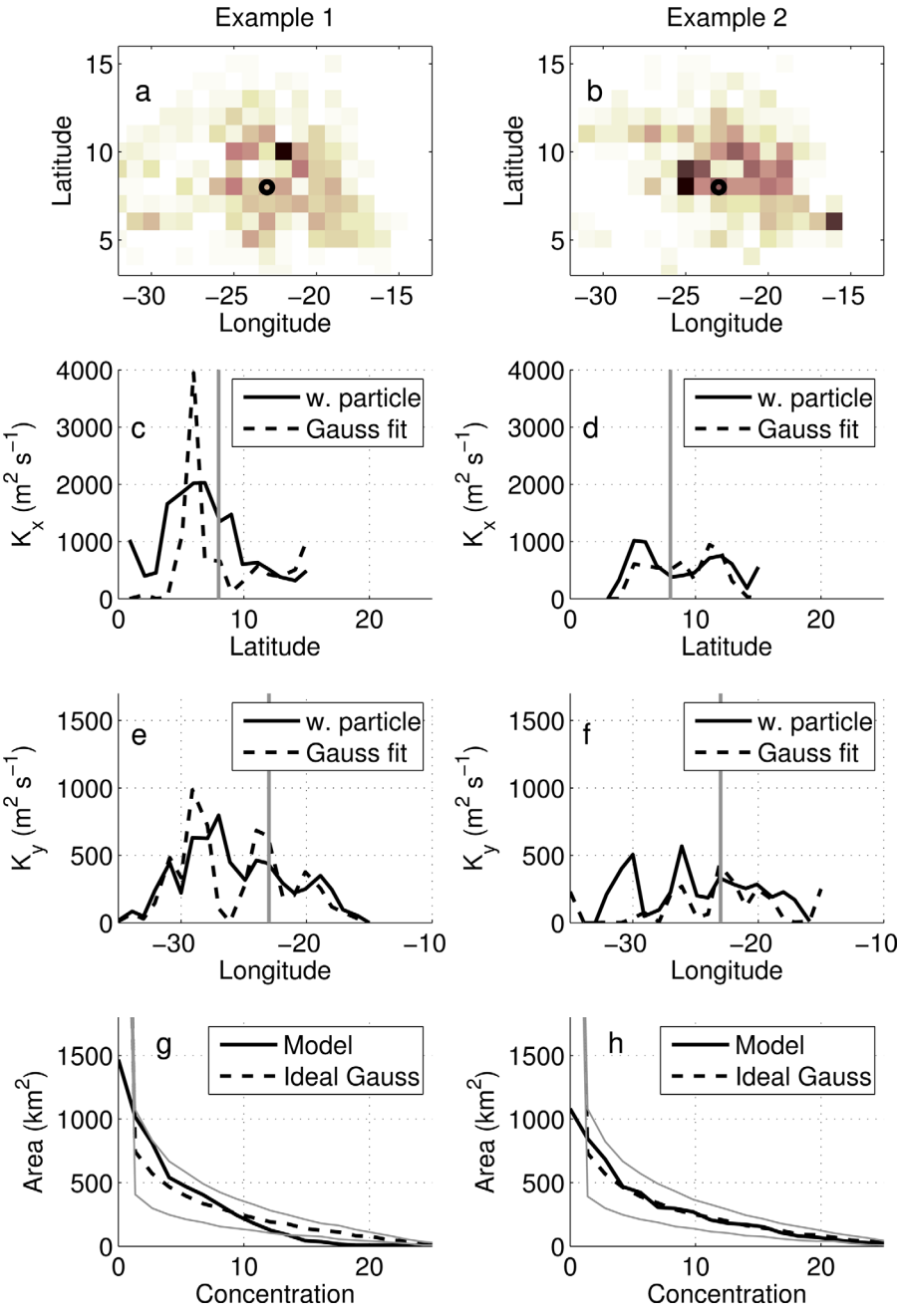

Figure 9. (a and b) Two random examples from the 53 synthetic tracer releases in FLAME model at a time period of 30 months sampled with the grid of 1°. The tracer release position is marked by a black circle. The (c and d) zonal and (e and f) meridional components of the eddy diffusivity are computed along each transect line. (g and h) Cumulative area-concentration function computed for the synthetic tracer release (thick black line) and its best fit computed for the isotropic Gaussian distribution (dashed line). Thin gray lines indicate the 100 m^2 s^{-1} deviation from the best estimate.

survey, which covered the zonal tracer expansion much better, resulted in a large zonal diffusivity estimate of about $K_x^{NI} = 1170$ m^2 s^{-1}.

[51] The diffusivity estimates for the interpolated data are larger as a consequence of smoothing. However, the interpolated data fill the gaps in the sampled area, hence, reduces noise in the estimates. The results are similar between the surveys for both zonal and meridional diffusivity components: $K_y^I \simeq 440$ m^2 s^{-1}, and $K_x^I \simeq 1100$ m^2 s^{-1}. In addition, the areal comparison method can be applied to the interpolated data. The estimated areal equivalent diffusivity is large, about 1000 m^2 s^{-1}, and is closer to the zonal K_x estimate, instead of the meridional K_y.

[52] To evaluate the computed lateral diffusivity components in GUTRE and to judge on their uncertainty, GUTRE's sampling strategy was applied to each of the 53 simulated tracer releases in FLAME model. For a noninterpolated data set, the meridional diffusivity (K_y^{g20} and K_y^{g30})

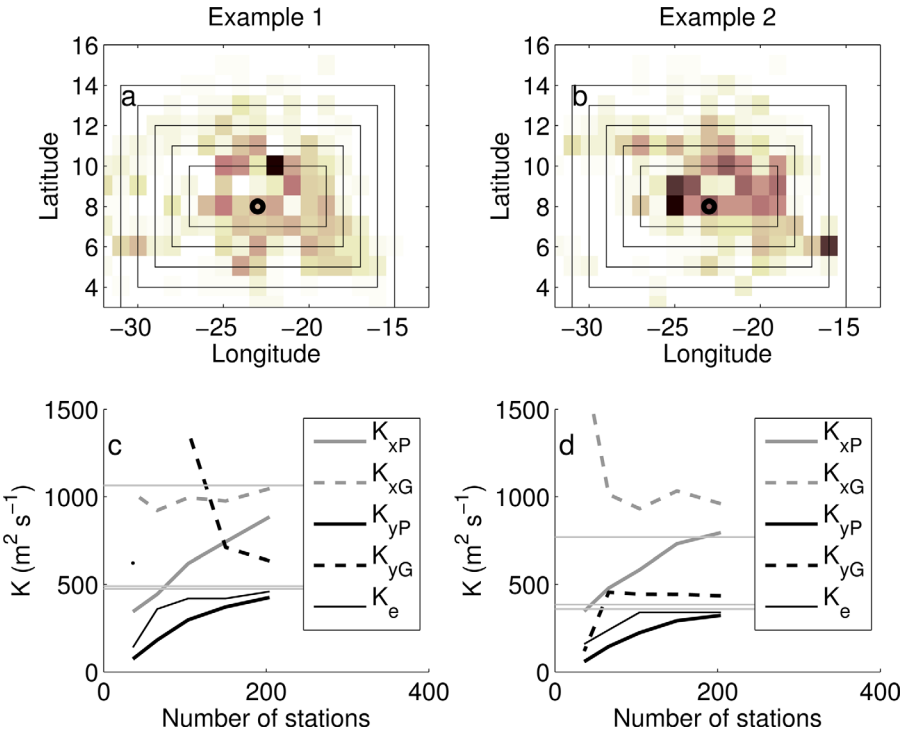

Figure 10. Eddy diffusivities computed when a sampled area is limited (black rectangles) for the same two examples as in Figure 9. The number of stations, using 1° sampling grid, are counted in each of the bounded areas. Three parallel gray lines in (c and d), from top to bottom, indicate the mean estimates of the full data set of K_x, K_e, and K_y, respectively. The eddy diffusivity computation methods are weighted particle (e.g., K_{xP}), Gaussian fit (e.g., K_{xG}), and areal comparison (K_e).

is about 40% smaller than the result obtained using a fine grid and full data set (K_y^f) as is shown in Figure 11 and Table 3. The zonal mixing coefficient (K_x^{g20}) is in a relatively good agreement with the full field estimates (K_x^f) for the sampling strategy of the second survey (20 months) in GUTRE. However, with the sampling strategy of the third survey, K_x^{g30} estimates are about three times (65%) smaller then the full data set estimates (K_x^f), which is an effect of limited westward extent of the third survey. Thus, FLAME model simulations indicate that GUTRE sampling strategy yields underestimated eddy diffusivities, when noninterpolated data sets are used.

[53] For the interpolated data set, the K_x^g and K_y^g estimates are almost in the range of uncertainties with the fine grid and full field estimates (K_x^f and K_y^f). The areal equivalent lateral diffusivity (K_e^g), on the other hand, is about 35% and 25% overestimated for the second and third surveys, respectively (Figure 12). We therefore expect a slight overestimation in GUTRE's K_e as well.

[54] Furthermore, it is worth to take a look into the results of several transect profiles done in each survey: along 8°N, 9°N, 25°W, and 21°W during the 20 months survey (Figure 13), and along 8°N, 10°N, 23°W, and 21°W during the 30 months survey (Figure 14). The model results indicate that a transect analysis can both overestimate and underestimate the true eddy diffusivity coefficients. However, even with the relatively frequent sampling achieved along the transects, the Gaussian fit is difficult to achieve. Nevertheless, meridional diffusivities are found to vary between 400 and 700 m^2 s^{-1} when applying both the

Table 3. Eddy Diffusivities Computed for GUTRE Second (20 Months) and Third (30 Months) Surveys, From Not Interpolated (NI) and Interpolated (I) Data, in Comparison to Lateral Diffusivities and Their Uncertainties Computed Using GUTRE Sampling Strategy for Each of the 53 Tracer Release Experiments in FLAME Model, From Interpolated (I) and Not Interpolated (NI) Data[a]

	20 m NI	GUTRE I	30 m NI	GUTRE I	20 m NI	FLAME I	30 m NI	FLAME I
K_{xP} (m^2 s^{-1})	1110	1050	530	980	640±40	980 ± 50	340 ± 20	680 ± 20
K_{xG} (m^2 s^{-1})	1230	1230	290	1260	940 ± 70	1190 ± 80	270 ± 20	850 ± 40
K_{yP} (m^2 s^{-1})	280	340	390	450	180 ± 20	320 ± 30	200 ± 20	270 ± 20
K_{yG} (m^2 s^{-1})	310	440	320	530	220 ± 20	380 ± 40	180 ± 20	320 ± 20
K_e (m^2 s^{-1})		1120		900		520 ± 30		450 ± 10

[a] K_{xP} and K_{yP} are eddy diffusivities from the weighted particle method, K_{xG} and K_{yG} are from the Gaussian fit method, and K_e is an areal equivalent lateral diffusivity.

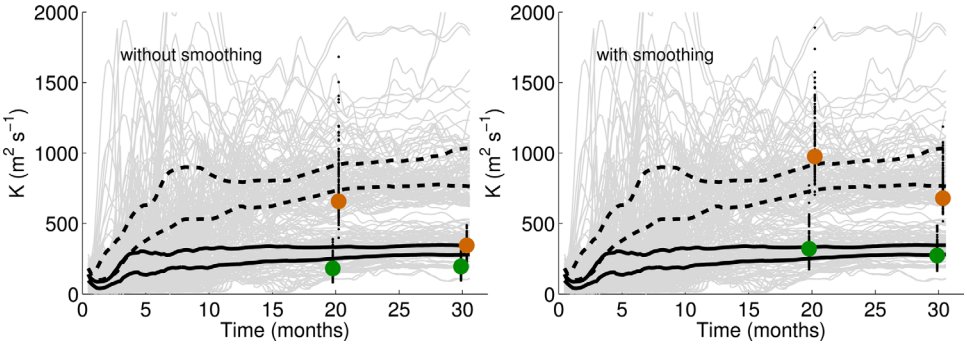

Figure 11. Eddy diffusivity estimates for each of the 53 tracer simulations in FLAME model, but with the sampling strategy of GUTRE at 20 and 30 months after tracer release: (left) not interpolated data set, (right) interpolated data set. The mean of each estimate is marked by a circle (brown for K_x estimates and green for K_y estimates) and slightly shifted in time. Both Gaussian fit and weighted particle methods are overplotted. Thin gray lines mark K_x and K_y estimates for each run as in Figure 7. Black solid lines mark the uncertainty ranges of mean K_y estimate, while black dashed lines mark the uncertainty ranges of mean K_x estimate.

Gaussian fit and the weighted particle methods. Zonal diffusivities vary between 1200 and 2500 m^2 s^{-1} from the Gaussian fit method and between 600 and 1500 m^2 s^{-1} from the weighted particle method. Considering large uncertainties in transect analysis, diffusivity estimates agree with both meridional and zonal GUTRE's results given above.

[55] In summary, the test of GUTRE's sampling strategy on FLAME model simulations yields that lateral diffusivity component for GUTRE data are slightly underestimated when Gaussian fit and weighted particle methods are used directly on spatially nonsmoothed data. We expect that such underestimation results from the sampling strategy used in two GUTRE's surveys. An arbitrary smoothing chosen for this study of Gaussian weights with the influence radius of 100 km, yields diffusivity estimates much closer to the full field estimates in FLAME test. Adjusting

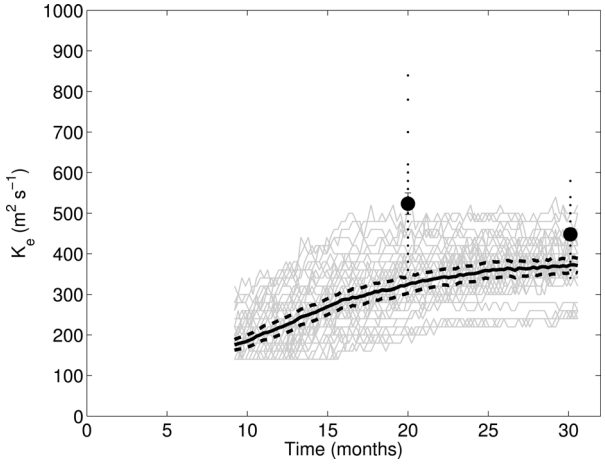

Figure 12. Areal equivalent lateral diffusivity for each of the 53 tracer simulations in FLAME model but with the sampling strategy of GUTRE after smoothing with Gaussian weights (black dots) and their mean (black circle). Thin gray lines mark K_e estimates for each experiment as in Figure 8.

GUTRE lateral diffusivity estimates in respect to the findings of FLAME model, we conclude that meridional diffusivity component in GUTRE is $K_y = 500 \pm 200$ m^2 s^{-1}, zonal$-K_x = 1200 \pm 600$ m^2 s^{-1}, and areal equivalent diffusivity $- K_e = 700 \pm 200$ m^2 s^{-1}. Here the uncertainty is twice the size of the uncertainties computed with the regular sampling grid of 2° in FLAME model, because we expect that the uncertainty increases with the irregular sampling grid.

5. Summary and Discussion

[56] The observations from the GUTRE were used to estimate spatially integrated lateral diffusivity components in meridional and zonal directions. Three methods were employed: Gaussian fit, weighted particle and areal equivalent, to estimate diffusivities. All of the methods and different sampling strategies were tested on two synthetic tracer releases: one using conceptual jet model of zonal jets and another one using high-resolution ocean model FLAME. The spatial scales of the tracer patch were about 1000 km in the meridional direction and 2000 km in the zonal direction, while time scales were between 20 and 30 months after tracer release from the "point" position. Hence, tracer patch, spread through almost the whole eastern basin of tropical North Atlantic, was not only governed by large-eddy dynamics, but was affected by possibly different eddy mixing regimes and alternating zonal jets. As a consequence, lateral diffusivity estimates are time and space integrated, where, additionally to the effect of eddies, the time-mean flow effects of zonal jets are also included.

[57] Our best estimate of meridional component of lateral diffusivity in the Guinea Upwelling region at about 300 m depth is $K_y = 500 \pm 200$ m^2 s^{-1}, and zonal $- K_x = 1200 \pm 600$ m^2 s^{-1}. In general, the pure advection by alternating zonal jets would yield higher zonal diffusivity component (K_x), when second moment of the tracer patch is evaluated. However, sheared flow also enhances tracer gradients and thus cross-flow tracer mixing. In this way, tracer patch diffusion in zonal direction is also enhanced. How well zonal tracer diffusion can be described

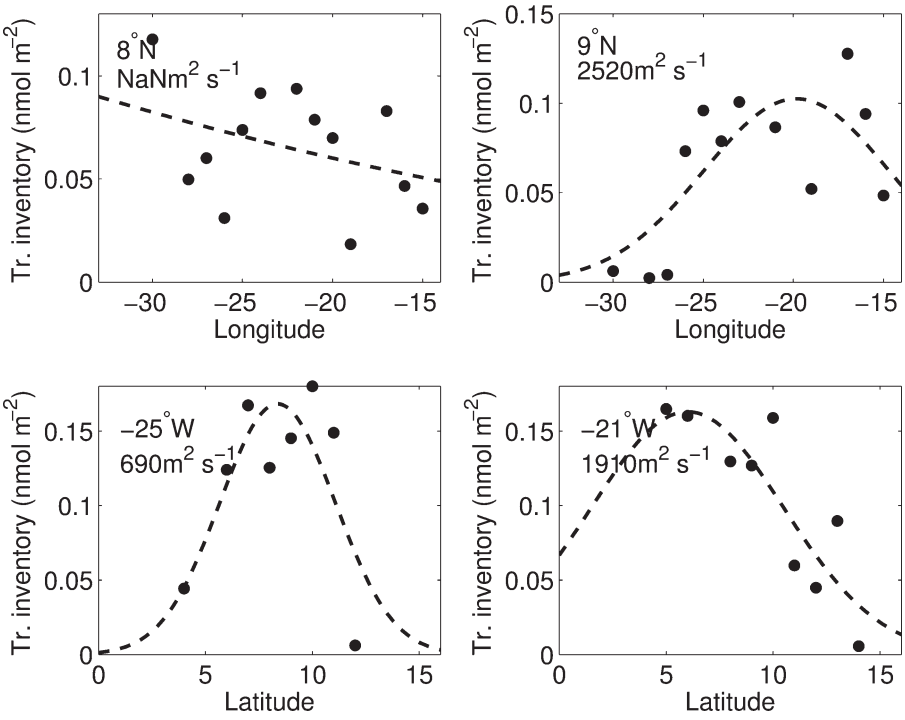

Figure 13. Gaussian distribution fit (dashed line) to four tracer patch transects along: 8°N, 9°N, 25°W, and 21°W (black dots), during the second GUTRE's survey (20 months).

by zonal mixing coefficient, as opposed to the pure shear of the tracer patch, can be quantified by using areal equivalent method. The areal equivalent tracer mixing coefficient in zonal direction is estimated to be $K_x^e = 1000 \pm 500$ m^2 s^{-1}. We therefore propose that tracer dispersion over large spatial scales by the complicated system of alternating zonal jets and eddies in the eastern tropical north Atlantic can be approximated by simple diffusion with asymmetric mixing coefficients: meridional $K_y \sim 500$ m^2 s^{-1} and zonal $K_x^e \sim 1000$ m^2 s^{-1}.

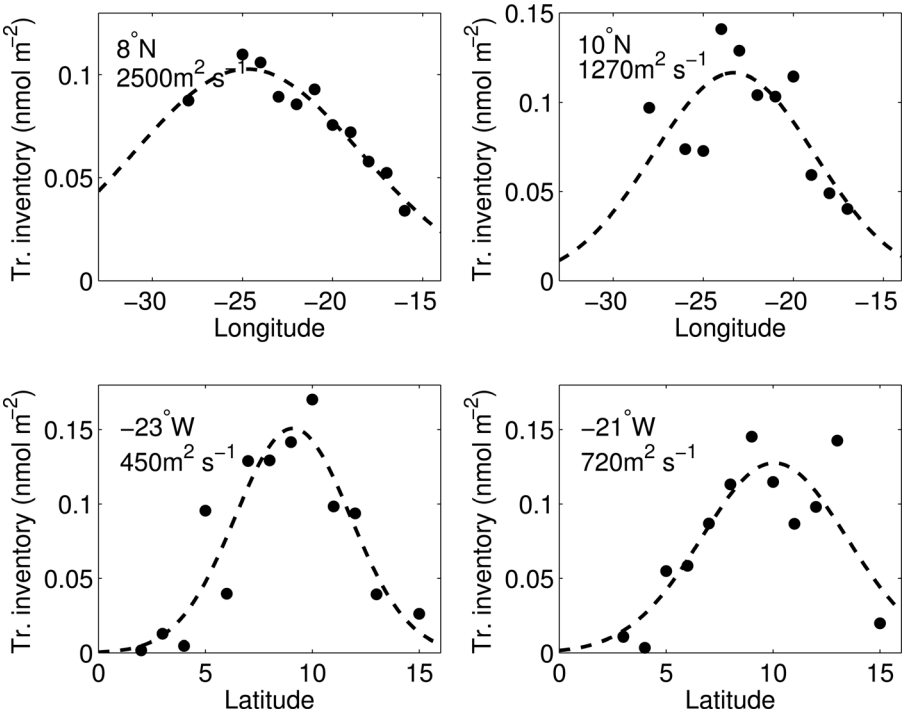

Figure 14. Gaussian distribution fit (dashed line) to four tracer patch transects along: 8°N, 10°N, 23°W, and 21°W (black dots), during the third GUTRE's survey (30 months).

[58] Our study method did not allow to separate eddy from zonal jet effects on the tracer spread. However, we looked at the question how large mean advection in our "toy"'-jet model is required to explain the anisotropy observed in lateral diffusion coefficients. The model takes into account the alternating time-mean flow and isotropic eddies, which we had chosen to be equal to the cross-mean-flow diffusivity estimate of $K_y = 500\ m^2\ s^{-1}$. The resulting velocity at the center of each jet is estimated to be $0.015 \pm 0.005\ m\ s^{-1}$. The obtained velocities are about twice smaller than the observations: *Brandt et al*. [2010] reports typical zonal jet velocities of about $0.03\ m\ s^{-1}$ at about 400 m in the tropical Atlantic. However, zonal jets as well as NEUC and NECC currents are varying both in space and time, whereas our "toy"-jet model is a great simplification of the mean-flow in the region. Overall, the tracer release experiment does not allow to differentiate how much of tracer dispersion is attributed to shear dispersion by zonal jets or to eddy mixing. The further complication is imposed by reported anisotropy of eddies, especially, in the tropical Atlantic from high-resolution model simulations [*Eden and Greatbatch*, 2009]. Both high-resolution model simulations and their comparison to observations are needed for a detailed evaluation of mean-flow-eddy processes in the region.

[59] GUTRE results can be compared to the results of the NATRE [*Ledwell et al*., 1998] carried out in the neighboring region to the north, at about 25°N and at the depth of about 300 m. The tracer release experiment was accompanied by the release of subsurface floats [*Sundermeyer and Price*, 1998]. The lateral diffusivity estimates in meridional direction were: $650\ m^2\ s^{-1}$ (200–1200) from the tracer and $700 \pm 400\ m^2\ s^{-1}$ from the floats. Zonally, the estimates were larger: $2300\ m^2\ s^{-1}$ (1000–4000) from the tracer and $1500 \pm 700\ m^2\ s^{-1}$ from the floats. In comparison to the NATRE results, GUTRE results agree better with the NATRE estimates derived from subsurface floats, but overall are about 20–30% smaller. In general, meridional eddy diffusivities in the tropical ocean are suggested to be smaller, influenced by zonal energy radiation by Rossby waves [*Eden and Greatbatch*, 2009]. The other process leading to the difference in results between the GUTRE and NATRE site, the latter of which is situated in the westward return flow of subtropical gyre is reported by [*Abernathey and Marshall*, 2013]. They have shown that in the westward mean flow the cross-flow diffusivities are larger, as a counterpart of the suppression of eddies by the mean eastward flow. Do the above mentioned processes fully explain the differences between observations of the two tracer release experiments needs yet to be shown.

[60] Finally, a short note on the sampling strategies of the tracer patch with the purpose to estimate lateral diffusivity. The comparison of high-resolution model simulations and observations allowed to search for the optimal sampling strategy in this study. We find that more than 70% of the tracer patch must be sampled to obtain diffusivity estimates with an uncertainty smaller than 50%. However, both 1° and 2° regular sampling grids yielded similar results when sampled the region of the same size. Hence, we conclude that lateral diffusivity estimates are more affected by a contraction of the sampled area than by a reduction in the horizontal sampling frequency.

[61] **Acknowledgments.** We would like to thank all persons involved in the measurement of the tracer as well as the captains, crews, and technicians on R/V Maria S. Merian and R/V Meteor and their home institutions for their support. Support for this work came from Deutsche Forschungsgemeinschaft as part of the Sonderforschungsbereich 754 "Climate-Biogeochemistry Interactions in the Tropical Ocean."

References

Abernathey, R., and J. Marshall (2013), Global surface eddy diffusivities derived from satellite altimetry, *J. Geophys. Res.*, *117*, 901–916, doi:10.1002/jgrc.20066.

Abernathey, R., J. Marshall, M. Mazloff, and E. Shuckburgh (2010), Critical layer enhancement of mesoscale eddy stirring in the Southern Ocean, *J. Phys. Oceanogr.*, *40*, 170–184.

Banyte, D., T. Tanhua, M. Visbeck, D. W. R. Wallace, J. Karstensen, G. Krahmann, A. Achneider, L. Stramma, and M. Dengler (2012), Diapycnal diffusivity at the upper boundary of the tropical North Atlantic oxygen minimum zone, *J. Geophys. Res.*, *117*, C09016, doi:10.1029/2011JC007762.

Berloff, P., I. Kamenkovich, and J. Pedlosky (2009), A model of multiple zonal jets in the oceans: Dynamical and kinematical analysis, *J. Phys. Oceanogr.*, *39*, 2711–2734.

Brandt, P., and C. Eden (2005), Annual cycle and interannual variability of the middepth tropical Atlantic Ocean, *Deep Sea Res., Part I*, 52, 199–219.

Brandt, P., V. Hormann, A. Körtzinger, M. Visbeck, G. Krahmann, and L. Stramma (2010), Changes in the ventilation of the oxygen minimum zone of the tropical north Atlantic, *J. Phys. Oceanogr.*, *40*, 1784–1801.

Dengg, J., C. Böning, U. Ernst, R. Redler, and A. Beckmann (1999), Effects of an improved model representation of overflow water on the subpolar North Atlantic, *Int. WOCE Newsl.*, *37*, 10–15.

Eden, C., and C. Böning (2002), Sources of eddy kinetic energy in the Labrador Sea, *J. Phys. Oceanogr.*, *32*, 3346–3363.

Eden, C., and R. J. Greatbatch (2009), A diagnosis of isopycnal mixing by mesoscale eddies, *Ocean Modell.*, *27*, 98–106.

Ferrari, R., and M. Nikurashin (2010), Suppression of eddy diffusivity across jets in the Southern Ocean, *J. Phys. Oceanogr.*, *40*, 1501–1519.

Fischer, T. (2007), *Simulating a tracer release experiment in the tropical east Atlantic ocean, diploma thesis*, Christian-Albrechts Univ., Kiel, Germany.

Fischer, T., D. Banyte, P. Brandt, M. Dengler, G. Krahmann, T. Tanhua, and M. Visbeck (2012), Diapycnal oxygen supply to the tropical North Atlantic oxygen minimum zone, *Biogeosci. Discuss.*, *9*, 14,291–14,325.

Garrett, C. (1983), On the initial streakiness of a dispersing tracer in two- and three-dimensional turbulence, *Dyn. Atmos. Oceans*, *7*, 265–277.

Gill, A. E., J. S. A. Green, and A. J. Simmons (1974), Energy partition in the large-scale ocean circulation and the production of mid-ocean eddies, *J. Mar. Res.*, *21*, 499–528.

Hüttl, S., and C. Böning (2006), Mechanisms of decadal variability in the shallow subtropicaltropical circulation of the Atlantic Ocean: A model study, *J. Geophys. Res.*, *111*, C07011, doi:10.1029/2005JC003414.

Hüttl-Kabus, S., and C. Böning (2008), Pathways and variability of the offequatorial undercurrents in the Atlantic Ocean, *J. Geophys. Res.*, *113*, C10018, doi:10.1029/2007JC004700.

Karstensen, J., L. Stramma, and M. Visbeck (2008), Oxygen minimum zones in the eastern tropical Atlantic and Pacific Oceans, *Prog. Oceanogr.*, *77*, 331–350.

Kamenkovich, I., P. Berloff, and J. Pedlosky (2009), Anisotropic material transport by eddies and eddy-driven currents in a model of the North Atlantic, *J. Phys. Oceanogr.*, *39*, 3162–3175.

Kirchner, K., M. Rhein, C. Martens, C. Böning, and S. Hüttl (2008), Observed and modeled meridional overturning circulation related flow into the Caribbean, *J. Geophys. Res.*, *113*, C03028, doi:10.1029/2007JC004320.

Kirchner, K., M. Rhein, S. Hüttl, and C. Böning (2009), On the spreading of South Atlantic water into the northern hemisphere, *J. Geophys. Res.*, *114*, C05019, doi:10.1029/2008JC005165.

Klocker, A., R. Ferrari, J. H. LaCasce, and S. T. Merrifield (2012), Reconciling float-based and tracer-based estimates of eddy diffusivities, *J. Mar. Res.*, *70*, 569–602.

Ledwell, J. R., A. J. Watson, and C. S. Law (1998), Mixing of a tracer in the pycnocline, *J. Geophys. Res. 103*, 21499–21529.

Luyten, J. R., J. Pedlosky, and H. Stommel (1983), The ventilated thermocline, *J. Phys. Oceanogr.*, *13*, 292–309.

Maximenko, N., B. Bang, and H. Sasaki (2005), Observational evidence of alternating zonal jets in the world ocean, *Geophys. Res. Lett.*, *32*, L12607, doi:10.1029/2005GL022728.

Nakano, H., and H. Hasumi (2005), A series of zonal jets embedded in the broad zonal flows in the Pacific obtained in eddy-permitting ocean general circulation models, *J. Atmos. Sci.*, *35*, 474–488.

Pacanowski, R., (1995), MOM2 documentation, user's guide and reference manual, Tech. Rep., 329 pp., Geophys. Fluid Dyn. Lab., Princeton, N. J.

Rhines, P. (1994), Jets, *Chaos*, *4*, 313–339.

Rypina, I. I., I. Kamenkovich, P. Berloff, and L. Pratt (2012), Eddy-induced particle dispersion in the near-surface, *J. Phys. Oceanogr.*, *42*, 2206–2228.

Smith, K. S. (2005), Tracer transport along and across coherent jets in two-dimensional turbulent flow, *J. Fluid Mech. 544*, 133–142.

Sundermeyer, M. A., and J. F. Price (1998), Lateral mixing and the North Atlantic tracer release experiment: Observations and numerical simulations of Lagrangian particles and a passive tracer, *J. Geophys. Res.*, *103*(C10), 21,481–21,497.

Sundermeyer, M. A., and M. P. Lelong (2005), Numerical simulations of lateral dispersion by the relaxation of diapycnal mixing events, *J. Phys. Oceanogr.*, *35*(C10), 2368–2386.

Stramma, L., S. Hüttl, and J. Schafstall (2005), Water masses and currents in the upper tropical Northeast Atlantic off northwest Africa, *J. Geophys. Res.*, *110*, C12006, doi:10.1029/2005JC002939.

Stramma, L., G. C. Johnson, J. Sprintall, and V. Mohrholz (2008), Expanding oxygen-minimum zones in the tropical oceans, *Science*, *320*, 655–658.